

Fe I in the Beta Pictoris circumstellar gas disk

II. The time variations in the iron circumstellar gas

F. Kiefer^{1,2}, A. Vidal-Madjar^{1,2}, A. Lecavelier des Etangs^{1,2}, V. Bourrier³, D. Ehrenreich³, R. Ferlet^{1,2},
G. Hébrard^{1,2}, and P. A. Wilson^{1,2,4}

¹ CNRS, UMR 7095, Institut d'Astrophysique de Paris, 98^{bis} boulevard Arago, F-75014 Paris, France

² UPMC Univ. Paris 6, UMR 7095, Institut d'Astrophysique de Paris, 98^{bis} boulevard Arago, F-75014 Paris, France

³ Observatoire de l'Université de Genève, 51 chemin des Maillettes, 1290, Sauverny, Switzerland

⁴ Department of Physics, University of Warwick, Coventry, CV4 7AL

ABSTRACT

β Pictoris is a young planetary system surrounded by a debris disk of dust and gas. The gas source of this disk could be exocomets (or “falling and evaporating bodies”, FEBs), which produce refractory elements (Mg, Ca, Fe) through sublimation of dust grains at several tens of stellar radii. Nearly 1700 high resolution spectra of β Pictoris have been obtained from 2003 to 2017 using the HARPS spectrograph. In paper I, we showed that a very high S/N ratio allows the detection of many weak Fe I lines in more than ten excited levels, and we derived the physical characteristics of the iron gas in the disk. The measured temperature of the gas (~ 1300 K) suggested that it is produced by evaporation of grains at about 0.3 au ($38 R_*$) from the star. Here we describe the yearly variations of the column densities of all Fe I components (from both ground and excited levels). The drop in the Fe I ground level column density after 2011 coincides with a drop in Fe I excited levels column density, as well as in the Ca II doublet and a ground level Ca I line at the same epoch. All drops are compatible together with photoionisation-recombination equilibrium and β Pic like relative abundances, in a medium at 1300 K and at 0.3 au from β Pictoris. Interestingly, this warm medium does not correlate with the numerous exocomets in the circumstellar environment of this young star.

Key words. Stars: Individual: Beta Pictoris; Circumstellar disk; Exocomets.

1. Introduction

The β Pictoris system is particularly famous for harboring one the most massive debris disk in the close neighborhood of the Sun (Smith & Terrile 1984). Despite being 20 Myr old (Mamaĵek & Cameron 2014), this star has gone through the phase of dissipating dust and gas in its protoplanetary disk, which remnant should be a gas-poor dust-poor debris disk. Observations however show that the disk is one of the most dusty gas-poor disk among known debris disk (Artymowicz et al. 1997, Vidal-Madjar et al. 1998). With the age of β Pictoris being much larger than typical timescales of destruction of dust particles (< 1 Myr), this led to the conjecture that a replenishment from either collisions or evaporation of hidden planetesimals was necessary to explain the overabundance of dust in this system (Backman & Paresce 1993, Lecavelier et al. 1996).

Moreover, absorption spectroscopy of β Pic revealed the presence of a stable gas component at the star’s radial velocity and variable absorptions attributed to transiting star-grazing exocomets (Ferlet et al. 1987, Beust et al. 1990) ; see also the review of Vidal-Madjar et al. (1998). The origin of the stable gas disk is still unknown, although highly suspected to be connected to the star-grazing exocomets that strongly evaporate dust and ionized species. Exocomets might be the common vector of gas and dust replenishment

in the disk of β Pictoris (Weissman 1984, Lecavelier et al. 1996, Li et al. 1998).

β Pictoris was observed with the HARPS instrument (see *e.g.* Pepe et al. 2011) for several years, from 2003 to 2017 thanks to large programs of follow-up (Lagrange et al. 2012, Kiefer et al. 2014, Lagrange et al. 2018). Thousands of spectra were gathered and several hundreds of exocometary events detected (Kiefer et al. 2014). In Paper 1 (Vidal-Madjar et al. 2017, VM17 hereafter), stacking the 1686 HARPS spectra collected between 2003 and 2015, we presented the measurements of the physical properties of the iron gas from the detection of a large number of Fe I absorption lines, from the ground level up to the 12969 cm^{-1} excited level. We concluded that the measured temperature of the gas (~ 1300 K) coincides with the sublimation temperature of iron from solid compounds, and therefore that this gas is likely produced by the evaporation of grains at about $38 R_*$ or 0.32 au from the star. Moreover, the ground level absorption lines of Fe I presented evidences of two components at different radial velocities. The component centred on the same radial velocity as the one found for the excited levels at $20.41 \pm 0.05 \text{ km s}^{-1}$ for which we derived the temperature of 1300 K, and a blueshifted component at $20.07 \pm 0.02 \text{ km s}^{-1}$.

Independently, Welsh & Montgomery (2016) found that the ground level Fe I absorption lines in the same β Pic HARPS spectra were experiencing a strong drop of equivalent width between 2011 and 2013. They proposed that the

Send offprint requests to: F. Kiefer (e-mail: flavien.kiefer@iap.fr)

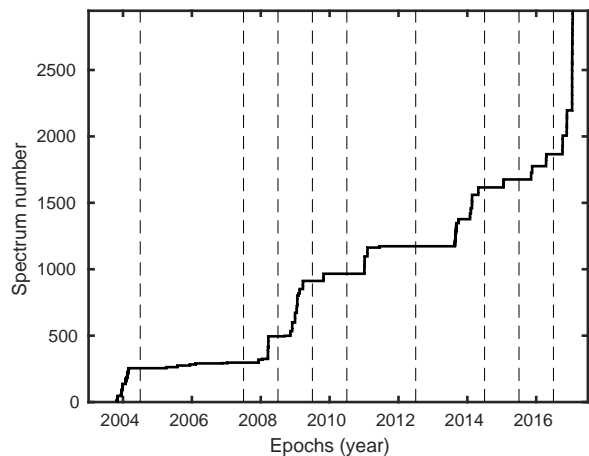


Fig. 1. The time distribution of the HARPS observing nights used in our study. The horizontal dotted lines show the limits of the selected observing periods.

source of the FeI experiencing the drop is the "D-family" of exocomets identified in Kiefer et al. (2014). These exocomets are composed of strongly evaporating bodies lying about a common orbit, with heliocentric radial velocities in the range $+20$ to $+50$ km s $^{-1}$.

Here we explore in more details the time variations of both ground and excited levels absorptions of FeI in the "stable" circumstellar medium, and how they correlate with exocomet activity in the vicinity of the star.

The analysis is presented in Sect. 3. The discussions and conclusion are given in Sect. 4 and 5, including a study on the variations also observed in the Ca II doublet (at 3934 and 3968 Å) and the Ca I line (at 4227 Å).

2. Observations

β Pictoris has been observed with the HARPS spectrograph mounted on the 3.6m telescope of La Silla (ESO Chile) from 2003 to 2017 on a (mostly) regular basis (except between 2004 and 2007 and in 2012). Since β Pictoris is observable only during summer in southern hemisphere, the observations were done essentially from September to April of each season. The 1D-spectra were extracted via the standard, most recent, HARPS pipeline (DRS 3.5) including localization of the spectral orders on the 2D-images, optimal order extraction, cosmic-ray rejection, wavelength calibration, flat-field corrections, and 1D-reconnection of the spectral orders after correction for the blaze. More details can be found in VM17. We organized the spectra into different samples, each constituting one summer of observation, with the exception of the period 2004-2007. During this period, the average number of spectra observed per summer was 14, which is very small compared to the other periods average (234 spectra per summer). For that reason we created a special sample covering the 3 summers from 2004 to 2007. This repartition is summarized in Table 1 and Fig. 1.

Because of the high S/N ratio achieved, we were able to detect numerous FeI absorption lines of the ground level, as well as, of several excited levels. All the detected FeI lines are listed in Table 2. The energy of the initial electronic levels of the corresponding transitions are summarized in Table 3. In the paper we always refer to the individual levels by their energy expressed in cm $^{-1}$, as e.g. FeI $_{416}$ for the

Table 1. The repartition of the 2946 HARPS observations. The signal-to-noise is calculated next to the main Fe I line between 3859.30 Å and 3859.70 Å.

Periods (year)	N_{obs}	N_{night}	Δt_{span} (day)	SNR (3860 Å)	Average Epoch
2003-2004	255	53	127	962	2004.025
2004-2007	42	14	651	390	2006.235
2007-2008	198	12	108	492	2008.203
2008-2009	417	12	196	909	2009.070
2009-2010	54	1	1	278	2009.847
2010-2011	207	4	159	467	2011.081
2013-2014	453	19	250	799	2013.929
2014-2015	60	4	4	493	2015.091
2015-2016	190	4	162	591	2016.063
2016-2017	1080	11	109	639	2017.041

Table 2. Transition parameters for the detected FeI lines, (i lower level, k upper level. A is the transition probability in s $^{-1}$, f is the oscillator strength, and E is the energy in cm $^{-1}$).

FeI lines (Å)	A_{ki} (s $^{-1}$)	f_{ik}	E_i (cm $^{-1}$)	E_k (cm $^{-1}$)
3795.002	1.15×10^7	3.47×10^{-2}	7986	34329
3799.547	7.31×10^6	2.04×10^{-2}	7728	34040
3812.964	7.91×10^6	1.23×10^{-2}	7728	33947
3815.840	1.12×10^8	1.90×10^{-1}	11976	38175
3820.425	6.67×10^7	1.20×10^{-1}	6928	33096
3824.443	2.83×10^6	4.83×10^{-3}	0	26140
3825.881	5.97×10^7	1.02×10^{-1}	7377	33507
3827.822	1.05×10^8	1.65×10^{-1}	12561	38678
3834.222	4.52×10^7	7.13×10^{-2}	7728	33802
3840.437	4.70×10^7	6.24×10^{-2}	7986	34017
3841.047	1.36×10^8	1.80×10^{-1}	12969	38996
3849.966	6.05×10^7	4.49×10^{-2}	8155	34122
3856.371	4.64×10^6	7.39×10^{-3}	416	26340
3859.911	9.69×10^6	2.17×10^{-2}	0	25900
3865.523	1.55×10^7	3.47×10^{-2}	8155	34017
3878.573	6.17×10^6	8.36×10^{-3}	704	26479
3886.282	5.29×10^6	1.20×10^{-2}	416	26140
3895.656	9.39×10^6	7.13×10^{-3}	888	26550
3899.707	2.58×10^6	5.89×10^{-3}	704	26340
3906.479	8.32×10^5	1.90×10^{-3}	888	26479
3920.257	2.60×10^6	1.79×10^{-2}	978	26479
3922.911	1.08×10^6	3.19×10^{-3}	416	25900
3927.919	2.60×10^6	1.00×10^{-2}	888	26340
3930.296	1.99×10^6	6.46×10^{-3}	704	26140
4045.812	8.62×10^7	2.12×10^{-1}	11976	36686
4063.594	6.65×10^7	1.65×10^{-1}	12561	37163
4071.738	7.64×10^7	1.90×10^{-1}	12969	37521
4271.760	2.28×10^7	7.62×10^{-2}	11976	35379
4307.902	3.38×10^7	1.21×10^{-1}	12561	35768
4325.762	5.16×10^7	2.03×10^{-1}	12969	36079
4383.544	5.00×10^7	1.76×10^{-1}	11976	34782
4404.750	2.75×10^7	1.03×10^{-1}	12561	35257

first excited level at 416 cm $^{-1}$. We will collectively refer to the excited levels as FeI $_{\text{Exc}}$, as opposed to the ground level FeI $_0$.

The profile of a few individual lines can be found in paper I, where we also describe the fitting procedure to derive the column densities, velocities and turbulent parameter.

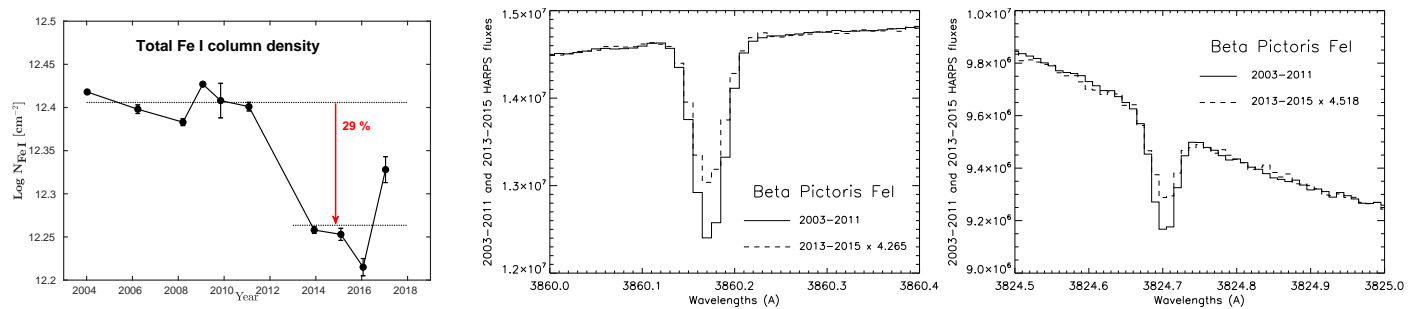


Fig. 2. Column density variations in the ground state of the circumstellar Fe I of β Pic. **Left:** Temporal variations of the total Fe I₀ column density showing a 30 % drop after year 2011. **Middle and right:** Sum of the Fe I HARPS fluxes, over the two separate periods, from 2003 to 2011 (solid) and after 2011 (dashed) at the ground state Fe I transition lines wavelengths, 3860 Å (middle) and 3824 Å (right).

Table 3. Fe I initial levels of the 32 electronic transitions detected in absorption in the HARPS spectrum of β Pictoris.

Energy level (cm^{-1})	Energy level (K)	J	Number of lines
0	0	4	2
416	598	3	3
704	1013	2	3
888	1278	1	3
978	1407	0	1
6928	9968	5	1
7377	10614	4	1
7728	11120	3	3
7986	11490	2	2
8155	11733	1	2
11976	17232	4	4
12561	18073	3	4
12969	18660	2	3

Table 4. Properties of the Fe I gas over the different epochs of observations, evaluated by fitting simultaneously the two absorption lines from the ground state (3859.30 Å and 3859.70 Å) with a single component.

Periods (year)	Nb. Obs.	v (km/s)	b (km/s)	$\log N_{\text{Fe I}}$ (cm^{-2})
2003-2004	215	20.15 ± 0.01	0.73 ± 0.02	12.418 ± 0.002
2004-2007	42	20.16 ± 0.02	0.81 ± 0.06	12.398 ± 0.005
2007-2008	198	20.20 ± 0.01	0.84 ± 0.04	12.383 ± 0.004
2008-2009	417	20.21 ± 0.01	0.77 ± 0.02	12.427 ± 0.002
2009-2010	54	20.22 ± 0.02	0.58 ± 0.13	12.408 ± 0.020
2010-2011	207	20.24 ± 0.02	0.93 ± 0.05	12.401 ± 0.005
2013-2014	453	20.14 ± 0.01	0.87 ± 0.03	12.258 ± 0.004
2014-2015	60	20.18 ± 0.02	0.85 ± 0.07	12.253 ± 0.007
2015-2016	190	20.16 ± 0.02	0.47 ± 0.08	12.215 ± 0.010
2016-2017	1080	20.20 ± 0.01	0.40 ± 0.05	12.328 ± 0.015

3. Temporal variations of Fe I circumstellar gas

3.1. Variation of the Fe I ground level

The time variation of the “stable” Fe I ground level absorption lines is given in Table 4, and plotted on Fig. 2. We fitted one single component for each separated period of observation, using the `Owens.f` code (Hébrard et al. 2002, Lemoine et al. 2002). It fits a Gaussian line-spread-function of 3.6 pixels wide, further broadened by a turbulent parameter b , centered on a radial velocity v and with depth fixed by the column density N and the levels transition parameters as given in Table 2. The continuum is fitted simultaneously using a 4-degree polynomial. The two Fe I lines of the ground level are plotted on Fig. 2.

The column density changes significantly, showing first a stable value of the order of $2.5 \cdot 10^{12} \text{ cm}^{-2}$ lasting about 7 years, followed by a 3.5σ drop down to about $1.8 \cdot 10^{12} \text{ cm}^{-2}$, lasting at least 4 years. This drop of about 30 % in the Fe I total column density was already noted by Welsh & Montgomery (2016) from the same HARPS observations. It seems that the column density is increasing again in 2017. Future observations should confirm this recent evolution.

The turbulent parameter b is stable up to a few hundreds of m s^{-1} indicating this gas ensemble is thermodynamically stable over nearly 12 years of observation. However, we observe a slow and monotonic reddening of the ground level

absorption over years up until 2011, followed by a sudden blueshift simultaneous to the column density drop. Thus the column density variation must be stronger in the red wing than on the blue wing of the Fe I line.

In the light of the two components model of VM17, it strongly suggests that only the reddest component at 20.4 km s^{-1} is experiencing the drop. Moreover, we show in the next section that a column density drop is also observed in the absorption lines of the excited levels that are centered on 20.4 km s^{-1} . We will revisit the Fe I ground level absorption lines analysis with a 2 components model in Section 3.3.

3.2. Variation of the Fe I excited levels

To further study the time behaviour of the Fe I source, we examine the variations of the Fe I excited levels absorption lines. These evaluations are given in Table 5, as calculated by fitting simultaneously all Fe I excited levels absorption lines with `Owens.f`. We fixed that the radial velocity and turbulent parameters $v_{\text{Fe I Exc}}$ and $b_{\text{Fe I Exc}}$ are common to all excited levels, while the column density can vary separately for each individual level. Only the strongest transitions show well distinguishable absorptions, since the noise wipes the weaker transition signatures away.

In VM17, we have observed for the whole 2003-2015 period that $v_{\text{Fe I Exc}} = 20.41^{+0.03}_{-0.05} \text{ km s}^{-1}$, and $b_{\text{Fe I Exc}} = 1.01 \pm 0.06 \text{ km s}^{-1}$. From Table 5 we can see

that in accordance to VM17, both the v and b of excited levels component remain stable in time about 20.39 km s^{-1} and 0.96 km s^{-1} respectively, except after 2014 where the velocity is more poorly determined. Conversely, the column densities from the excited levels present a time behaviour similar to the ground level with an important drop after 2011.

To have a better look at the column density variations of the excited levels, we plotted in Fig. 3 all excited levels values (and upper limits), compared to the ground level $N_{\text{FeI}0}^{\text{Total}}$ variations. The cleanest FeI_{416} and FeI_{6928} levels and the total column density in all excited levels are highlighted. All levels column densities are normalized to their corresponding median value before the drop, over the 2003 - 2011 period. To calculate the total column density and their uncertainties, we drew at each epoch 10^4 series of estimations of the column density at all excited levels according to their measurements distribution, then calculated the sum leading to 10^4 estimations of the total column density, and determined the final measurement as the median of the sample with errorbars as the $1-\sigma$ percentiles.

The drop observed on the total column density of the excited levels is significant at the $6-\sigma$ level, with an amplitude of $37 \pm 4\%$. It is larger for the excited levels than for the ground level, for which we measure a $31 \pm 2\%$ relative decrease in the column density, leading to a $2-\sigma$ significant difference in amplitude. This suggests again that only part of the ground level is undergoing the same drop than the excited levels.

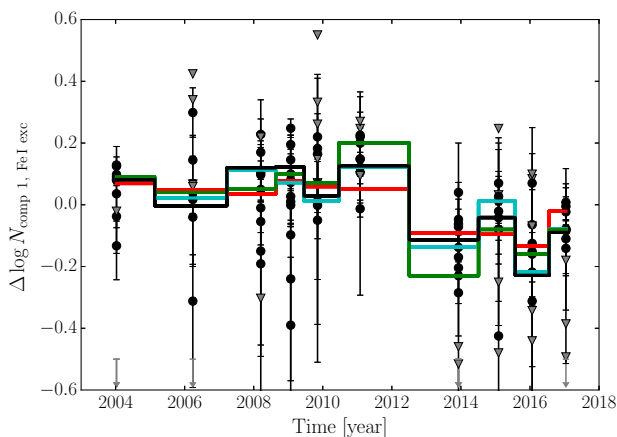


Fig. 3. The spread and evolution of the (log) Fe I column density among the 12 excited levels over time. The black circles refer to each excited level's column density relative to its median value as observed from 2003 to 2017. The grey triangles are upper limits derived from weaker absorptions. A few points outside the plot window are figured by arrows next to the axis. The black solid line shows how the total column density of excited Fe I varies over time. The cyan and green solid lines show the evolution of the column densities derived respectively for the FeI_{416} and FeI_{6928} excited levels. The FeI_0 variations derived in Table 4 are shown as a solid red line.

3.3. Revisiting the ground level variations with a 2 components model

It has been proposed by VM17 that the absorption lines of the ground level can be divided into 2 components, one of which, at about 20.4 km s^{-1} , is common with excited levels

transition lines, and a second one lying at about 20.0 km s^{-1} . In the rest of the paper, we will refer to these 2 hypothesized components as the *red component* and the *blue component* respectively. Besides the variations observed in the excited levels, additional clues suggest two components might be indeed present in the Fe I ground level lines.

First, as observed in section 3.1, the velocity variations of the one-component fit of the FeI_0 absorption lines show that simultaneously to the column density drop there is a blueward shift of the centroid wavelength, suggesting that only the red part of the lines undergoes a drop. Second, the amplitude of the drop in ground level column density is 2-sigma lower than the excited levels column density drop suggesting that only a part of the total amount of Fe I in ground level is vanishing. Revisiting the analysis of the FeI_0 absorption lines using a 2 components model should confirm these assertions.

From the fit of the excited levels absorption lines in Table 5, the radial velocity of the red component fluctuates about the average value $v_2 = 20.39 \text{ km s}^{-1}$, without any trend. We will thus assume that the red component radial velocity is constant and fix it to this value. We then proceed to a 2-components fit of the ground level absorption line, adding a new component and letting all parameters free except v_2 . The results are given in Table 6.

We find that the derived radial velocity of the blue component is weakly fluctuating around the average value $v_1 = 19.77 \text{ km s}^{-1}$. However, the derived turbulence parameters have strong scatters with values lower than 0.05 km s^{-1} for b_1 and as high as 1.5 km s^{-1} for b_2 . This is not surprising since we are fitting strongly blended features. Other parameters should be fixed to lower such overfitting effects.

We thus fix both radial velocities v_1 and v_2 to respectively 19.77 km s^{-1} and 20.39 km s^{-1} . This time the values of the turbulent parameters are better behaved, with $b_1 \sim 0.11 \pm 0.02 \text{ km s}^{-1}$ and $b_2 \sim 0.77 \pm 0.09 \text{ km s}^{-1}$. The two periods 2015-2016 and 2016-2017 stands aside: as for the excited levels the transition line is not well fit with the common model (for excited levels we measured $v \sim 20.20 \text{ km s}^{-1}$). This shift is likely to be imputed to the upgrade of the instrument done in June 2015¹. Fortunately, it does not impact the measurement of the column density, so the 2015-2017 period remains valuable for the present analysis.

The measured ground level column density variations in each component are plotted in Fig. 4. The column density of the blue component is found monotonically decreasing, while the red component undergoes a strong drop. This difference is especially pronounced between 2011 and 2013 during the drop, with the red component column density divided by a factor of 2, and the blue component remaining essentially stable. Interestingly, the red variations follow well the excited levels variations with a slight increase of column density between 2003 and 2011.

A Pearson's R test shows that the total excited levels column density calculated in Table 5 explains the variations of the red component with $R = 0.87$ (null-hypothesis rejection probability $p = 9.8 \cdot 10^{-4}$), while it only explains the variations of the blue component with $R = 0.59$ ($p = 0.074$). This means that the red component measurements, having also smaller errorbars (~ 0.02) than the blue component column

¹ <https://www.eso.org/sci/publications/messenger/archive/no.162-dec15/messenger-no162-9-15.pdf>.

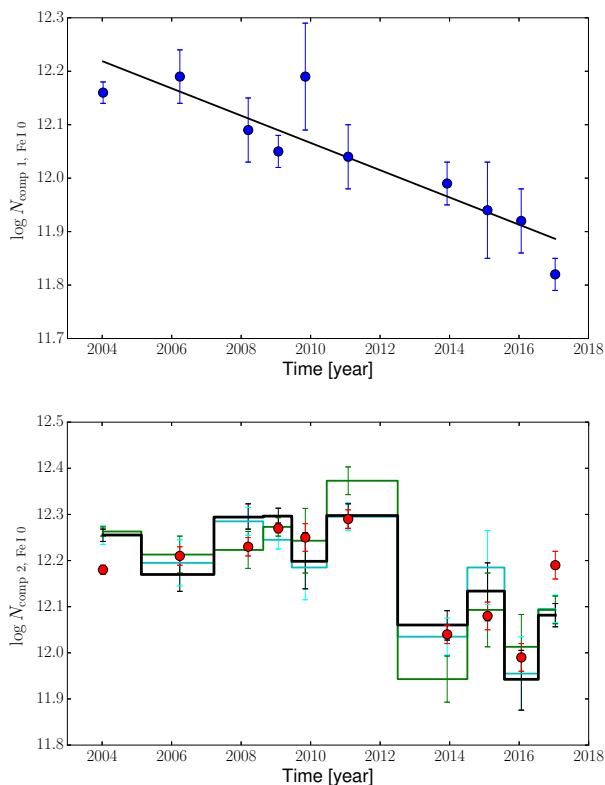


Fig. 4. Column density variations measured in the Fe I ground level absorption lines. Top panel: blue component at 19.80 km/s. The solid black line is a linear model fit of the data. Bottom panel: red component at 20.4 km/s. The coloured solid lines are the variations observed in excited levels column densities of Fe I₄₁₆ (cyan), Fe I₆₉₂₈ (green) and total excited Fe I (black), as given in Table 5. They are scaled up to ground level column density.

density (~ 0.06), are much better explained by the excited levels variations. However it is difficult to firmly conclude on the compatibility of the blue component column density variations with the excited levels, because although they have larger scatter, they also have larger measurement uncertainties.

Conducting another Pearson’s R test on linear relationship of the components column density with time shows that the blue component is better explained by a continuous decrease through the different epochs, with $R = -0.90$ ($p = 3.7 \cdot 10^{-4}$), while the red component has only $R = -0.56$ ($p = 0.093$).

The red and the blue are thus most likely uncorrelated, and the drop in the ground level column density is better explained, as initially suspected, by only the variation of a single component centered on 20.4 km s^{-1} . Observing this red component in the absorption lines of both excited and ground levels, and keeping in mind the measured temperature of this medium by VM17 (1300 K), leads to infer that the dropping component is located at close distance ($\sim 38 R_{\star}$) to the star and varies from a yet unknown process, perhaps exocomets activity drop, as proposed by Welsh & Montgomery (2016) and studied in more details in Section 4.

Since there is no evidence for a blue component in the excited levels lines, it should thus be located at larger dis-

tance to the star, certainly several AU where temperatures are much lower than 1000 K. This would explain the absence of a correlation with the inner red component. It is moreover strongly pushed-out in the anti-stellar direction, and slowly dissipating. This component might be part of the distant expanding circumstellar gas identified by Brandeker et al. (2004, 2011).

4. Exploring the link with β Pictoris circumstellar environment

4.1. Exocomets activity in the Ca II doublet

It has been suggested by Welsh & Montgomery (2016) and VM17 that the circumstellar (CS) Fe I originates from the numerous exocomets observed in the system of β Pictoris. One possible way to test this conjecture would be to determine if variations in the Fe I absorption lines of the circumstellar gas correspond to variations in the cometary activity, or the quantity of particles evaporated from these exocomets.

In the same HARPS spectra as those used here to analyse Fe I lines, there are the Ca II doublet lines that were used in Kiefer et al. (2014) to show that the β Pic’s exocomets separate into 2 families. The D-family would be composed of strongly evaporating comets about a common orbit, while the S-family would be composed of older comets with smaller amounts of gas released in the circumstellar medium. The D-family absorption signatures are all located within the -10 to 50 km s^{-1} range in the β Pic rest frame, while the S-family signatures are scattered on a wider velocity range, spanning from -100 to 150 km s^{-1} .

In order to quantify the cometary activity around β Pictoris, we can calculate the average absorption depth in different velocity domains of the Ca II normalized spectrum. In the small region about the tip of the circumstellar line that reaches almost zero, there could be deep features strongly blended with the circumstellar line; we thus first exclude that region from the analysis, within the range bounded by the instrument resolution ($\pm 2.6 \text{ km s}^{-1}$) about 21.57 km s^{-1} , the tip of the CS line close to the β Pic systemic velocity. We fixed the velocity domain for the D-family to be $+5$ - 25 km s^{-1} and for the S-family to be 50 - 100 km s^{-1} . These two domains are not overlapping and are centered on the core regions of each family detection statistics, as found in Kiefer et al. (2014).

The reference spectrum that is divided out of the spectra contains the stellar lines and the stable circumstellar and interstellar components. Thus, in the normalized spectra, only flux variations due to exocomet absorption or circumstellar disk fluctuations remain.

The average absorption depth (AAD, hereafter) is measured by averaging each normalized spectrum over the specified spectral band. It is thus proportional to the equivalent width, by a factor $\Delta\lambda$, the wavelength width of the calculation window. Therefore, as long as the absorbing medium is optically thin, this quantity reflects the amount of materials released in the circumstellar medium by transiting exocomets. It also provides information on the typical depth of signatures that are present in the spectrum within the velocity bounds.

Table 5. The temporal variations of the FeI excited levels in $v_{\text{FeI Exc}}$, heliocentric velocity (km/s), $b_{\text{FeI Exc}}$ value (km/s) and Log N column density (in Log cm^{-2} , identified by the energy level in cm^{-1}) evaluated by fitting simultaneously all excited levels absorption lines, epoch by epoch. The sum of the column density in all excited levels is given on the last line. The † sign individualizes the rows with the cleanest column density determination. Those are plotted as solid lines in Fig. 3.

Periods	2003-2004	2004-2007	2007-2008	2008-2009	2009-2010	2010-2011	2013-2014	2014-2015	2015-2016	2016-2017
Nb. Obs.	215	42	198	417	54	207	453	60	190	1080
$v_{\text{FeI Exc}}$	20.39±0.03	20.37±0.09	20.39±0.08	20.45±0.03	20.47±0.14	20.33±0.07	20.34±0.08	20.85±0.17	20.19±0.15	20.18±0.06
$b_{\text{FeI Exc}}$	0.80±0.10	0.78±0.33	1.20±0.20	0.98±0.09	1.00±0.53	1.22±0.17	0.89±0.29	1.47±0.51	1.14±0.54	1.00 (fixed†)
†log N _{FeI 416}	11.61±0.02	11.55±0.05	11.64±0.03	11.60±0.02	11.54±0.07	11.65±0.03	11.39±0.04	11.54±0.08	11.31±0.08	11.45±0.03
log N _{FeI 704}	11.25±0.03	10.84 ^{+0.15} _{-0.28}	11.38±0.05	11.40±0.03	11.15 ^{+0.15} _{-0.24}	11.30±0.08	11.09±0.08	11.11±0.15	10.84 ^{+0.16} _{-0.36}	11.16±0.06
log N _{FeI 888}	11.01±0.06	11.18±0.08	10.69 ^{+0.20} _{-0.30}	10.88±0.07	<10.96	11.03±0.10	10.81 ^{+0.11} _{-0.16}	10.86 ^{+0.20} _{-0.37}	10.73 ^{+0.20} _{-0.50}	10.74 ^{+0.12} _{-0.20}
log N _{FeI 978}	10.51 ^{+0.08} _{-0.12}	<10.47	<10.10	10.45 ^{+0.16} _{-0.29}	10.73 ^{+0.24} _{-0.57}	<10.65	10.50 ^{+0.12} _{-0.19}	<10.65	<10.06	<9.91
†log N _{FeI 6928}	10.92±0.01	10.87±0.04	10.88±0.04	10.93±0.02	10.90±0.07	11.03±0.03	10.60±0.05	10.75±0.08	10.67±0.07	10.75±0.03
log N _{FeI 7377}	10.47±0.03	10.49±0.08	10.45±0.09	10.54±0.03	10.51 ^{+0.13} _{-0.19}	10.45±0.09	10.06 ^{+0.10} _{-0.14}	9.92 ^{+0.31} _{-0.97}	10.22±0.20	10.34±0.06
log N _{FeI 7728}	<9.67	<10.74	10.83 ^{+0.17} _{-0.26}	10.27 ^{+0.22} _{-0.38}	10.88 ^{+0.19} _{-0.33}	<10.41	<9.80	<10.23	<10.40	<9.93
log N _{FeI 7986}	<9.90	<9.98	<10.14	9.87 ^{+0.18} _{-0.33}	<10.07	10.31 ^{+0.15} _{-0.24}	10.15 ^{+0.16} _{-0.26}	<9.67	<10.02	<9.10
log N _{FeI 8155}	<8.90	<10.15	9.95 ^{+0.25} _{-0.78}	10.18 ^{+0.10} _{-0.13}	<10.36	<10.08	<9.35	<9.33	10.17 ^{+0.18} _{-0.32}	<9.63
log N _{FeI 11976}	9.68 ^{+0.04} _{-0.05}	9.56 ^{+0.12} _{-0.16}	9.59 ^{+0.10} _{-0.12}	9.61 ^{+0.07} _{-0.08}	9.55 ^{+0.21} _{-0.46}	9.82±0.08	9.43 ^{+0.10} _{-0.15}	9.67±0.13	<9.11	9.49±0.12
log N _{FeI 12561}	9.24 ^{+0.07} _{-0.11}	<8.39	9.15 ^{+0.24} _{-0.40}	9.35 ^{+0.08} _{-0.10}	<9.48	9.43 ^{+0.14} _{-0.22}	9.00 ^{+0.19} _{-0.41}	<9.18	9.14 ^{+0.23} _{-0.46}	9.12 ^{+0.11} _{-0.43}
log N _{FeI 12969}	9.12 ^{+0.08} _{-0.11}	9.27 ^{+0.14} _{-0.21}	9.35 ^{+0.11} _{-0.16}	9.28 ^{+0.06} _{-0.09}	<9.44	9.24 ^{+0.16} _{-0.28}	<8.47	9.28 ^{+0.19} _{-0.34}	<9.11	9.23 ^{+0.14} _{-0.20}
†log N _{FeI Exc} ^{Total}	11.93±0.01	11.84±0.04	11.96±0.03	11.97±0.02	11.87±0.06	11.97±0.03	11.73±0.03	11.80±0.06	11.61±0.07	11.75±0.03

† The b-value was fixed at the median value from past measurements, because Owens.f was unable to converge on a realistic value.

Table 6. Table of fitting parameters, modelizing the FeI ground level absorption lines with 2 components.

Periods	2003-2004	2004-2007	2007-2008	2008-2009	2009-2010	2010-2011	2013-2014	2014-2015	2015-2016	2016-2017
Nb. Obs.	215	42	198	417	54	207	453	60	190	1080
<i>Comp 2 fixed to $v=20.39 \text{ km s}^{-1}$</i>										
$V_{\text{comp},1, \text{FeI } 0}$	19.48 ^{+0.11} _{-0.05}	20.08 ^{+0.05} _{-0.11}	19.72±0.20	19.73 ^{+0.15} _{-0.06}	19.84 ^{+0.15} _{-0.40}	19.81 ^{+0.04} _{-0.17}	19.48±0.10	19.96±0.11	19.85±0.20	19.78 ^{+0.20} _{-0.11}
$b_{\text{comp},1, \text{FeI } 0}$	0.04 ^{+0.02} _{-0.01}	0.16±0.05	<0.07	0.06±0.02	<0.09	<0.06	<0.05	0.09 ^{+0.06} _{-0.04}	<0.14	0.20 ^{+0.23} _{-0.14}
$b_{\text{comp},2, \text{FeI } 0}$	0.55 ^{+0.08} _{-0.04}	1.50 ^{+0.55} _{-0.28}	0.87 ^{+0.38} _{-0.10}	0.77±0.03	0.65 ^{+0.48} _{-0.20}	0.99±0.08	0.76 ^{+0.05} _{-0.08}	1.17 ^{+0.40} _{-0.20}	0.43 ^{+0.17} _{-0.13}	0.19 ^{+0.09} _{-0.03}
log N _{comp 1, FeI 0}	12.02±0.03	12.36±0.06	12.07 ^{+0.06} _{-0.12}	12.01±0.04	12.20 ^{+0.09} _{-0.30}	12.03 ^{+0.07} _{-0.12}	11.86±0.07	12.04 ^{+0.05} _{-0.15}	11.95 ^{+0.05} _{-0.15}	11.79±0.09
log N _{comp 2, FeI 0}	12.28 ^{+0.01} _{-0.03}	11.94 ^{+0.15} _{-0.11}	12.24 ^{+0.03} _{-0.16}	12.29 ^{+0.01} _{-0.06}	12.25 ^{+0.02} _{-0.08}	12.29±0.02	12.12±0.02	12.00 ^{+0.07} _{-0.14}	11.96±0.10	12.20 ^{+0.04} _{-0.11}
χ^2 (DOF=137)	142.86	143.03	142.63	154.14	139.22	140.21	144.99	142.70	138.39	137.85
<i>Comp. 1 fixed to $v=19.77 \text{ km s}^{-1}$</i>										
<i>Comp. 2 fixed to $v=20.39 \text{ km s}^{-1}$</i>										
$b_{\text{comp},1, \text{FeI } 0}$	0.14±0.02	0.06±0.02	0.05±0.03	0.08±0.02	<0.04	<0.04	0.08 ^{+0.04} _{-0.02}	<0.12	0.06 ^{+0.06} _{-0.03}	0.28±0.15
$b_{\text{comp},2, \text{FeI } 0}$	0.81±0.03	0.90±0.08	0.91±0.05	0.82±0.03	0.63±0.13	1.00±0.05	1.01±0.05	0.98±0.10	0.43±0.15	0.20 ^{+0.09} _{-0.03}
log N _{comp 1, FeI 0}	12.16±0.02	12.19±0.05	12.09±0.06	12.05±0.03	12.19±0.10	12.04±0.06	11.99±0.04	11.94±0.09	11.92±0.06	11.82±0.03
log N _{comp 2, FeI 0}	12.18±0.01	12.21±0.02	12.23±0.02	12.27±0.01	12.25±0.03	12.29±0.02	12.04±0.02	12.08±0.03	11.99±0.03	12.19±0.03
χ^2 (DOF=138)	153.79	147.04	143.11	156.63	139.24	140.23	149.60	143.93	138.39	137.87

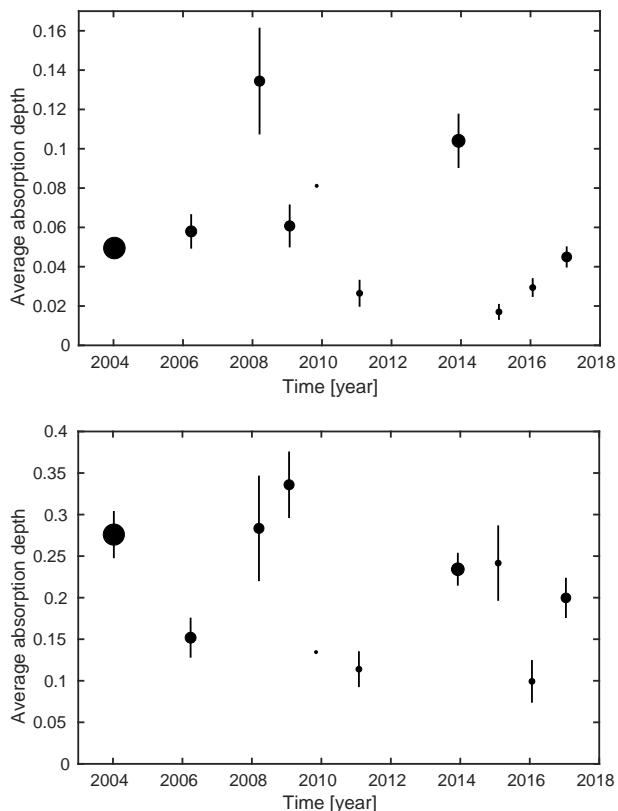


Fig. 5. Average absorption depth variations in the co-added Ca II K and H absorption spectra. **Top:** S-family, between 50 and 100 km s⁻¹. **Bottom:** D-family, between 5 and 25 km s⁻¹. The marker size is proportional to the number of nights where β Pic was observed by HARPS in each period (see Table 1). The errorbars indicate the scatter of average absorption depth during each period. See text for explanations.

Most of the time, several spectra are observed on the same night; this allows us to obtain an average AAD per night, a measure of exocometary activity during a single night. Averaging these night-based AAD over each of the periods considered in this paper (Table 1) we get a measure of how much the exocometary activity varies through time from one period to the other. It could then be compared to the Fe I variations in Fig. 4. Using the night-based AAD for this computation, rather than averaging over all spectra of a given period, makes more sense, because it prevents nights with many collected spectra to dominate the period-based AAD. These average absorption depth are plotted for each exocomet family on Figure 5.

As can be seen, there is no obvious long-term variations or sudden drop in the exocomet activity. On the contrary, the measurements scatter and the errorbars show that the total quantity of particles evaporated from the many transiting exocomets is variable even within a given period. Thus we see no evidence here for any correlation between exocomet activity and Fe I disk column densities.

4.2. Variability in the core of the Ca II CS line

We first excluded the strongly blended CS line region (0 ± 5 km s⁻¹), since we were initially interested in exocomet absorption. However, the CS line region incorporates cir-

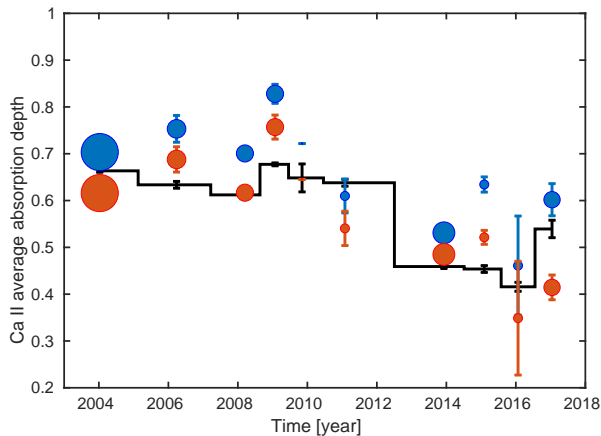


Fig. 6. Average absorption depth (AAD) variations in the Ca II circumstellar line region 0 ± 5 km s⁻¹. In blue, the K-line AAD and in red the H-line. They are compared to the total Fe I ground level column density variations in Table 4. The marker size is proportional to the number of nights where β Pic was observed by HARPS in each period (see Table 1). For the sake of comparison, the Fe I column densities are scaled to the Ca II AAD median.

cumstellar disk variations, as well as exocomets transit signatures. It is interesting to see if significant Ca II variations show up in that region, even though we are not able to know their origin. We plotted the AAD variation in this domain in Fig. 6.

This time, we observe a neat decrease in average absorption depth. The varying blended features in that region have an average depth of about 0.68 ± 0.03 in 2003-2011 and decrease to 0.50 ± 0.04 in 2013-2017, for a total 3.6σ drop of 26% along the 14 years of observations. This is comparable to the measured drop of column density of Fe I. This variation is confirmed by measuring a flux increase in the 5 pixels at the tip of the K-line from 0.0096 ± 0.0012 to 0.0196 ± 0.0021 in arbitrary unit, and from 0.0166 ± 0.0019 to 0.037 ± 0.0064 at the tip of the H-line.

Given that the average absorption depth is directly proportional to equivalent width, and thus at first approximation to average column density in the absorbing medium, we see that both Ca II medium and Fe I medium varied in about the same proportions. This has implications on the Fe and Ca relative abundance in the circumstellar medium close to the star, that we will explore in more details in the next section.

In conclusion, the variations experienced by the Fe I components column density are likely connected to Ca II variations in the circumstellar medium. Ca and Fe are thus part of a common reservoir that suddenly dissipated between 2011 and 2013. We cannot firmly identify the origin of these variations, which could be either large low-velocity exocomets or local gas disk inhomogeneities. The exocomets scenario is however less likely as they would have to be disconnected to the already known exocomets which families show no sign of long-term or sudden variations.

Table 7. The variation of the Ca II average absorption depth and average flux around Ca II K and H circumstellar lines. Average absorption depths are calculated from the normalized spectra, either separating K and H spectra, either co-adding the K and H absorption lines. Average fluxes are calculated from the raw spectra. Their continuum is scaled to an arbitrary level that is common to all spectra.

Periods	Average absorption depth				Average flux [arb. unit]		
	CS-line		D-family	S-family	tip of CS-line		blue wing
	K only $\pm 5 \text{ km s}^{-1}$	H only $\pm 5 \text{ km s}^{-1}$	K & H coadded 5 - 25 km s^{-1}	50 - 100 km s^{-1}	K only 0 $\pm 2 \text{ km s}^{-1}$	H only 0 $\pm 2 \text{ km s}^{-1}$	K only -150 $\pm 5 \text{ km s}^{-1}$
2003-2004	0.704 \pm 0.014	0.61597 \pm 0.010	0.276 \pm 0.028	0.0495 \pm 0.0045	0.01118 \pm 0.00063	0.01843 \pm 0.00062	0.3881 \pm 0.0010
2004-2007	0.753 \pm 0.029	0.68788 \pm 0.027	0.152 \pm 0.024	0.0580 \pm 0.0088	0.0105 \pm 0.0016	0.0162 \pm 0.0024	0.3864 \pm 0.0024
2007-2008	0.701 \pm 0.013	0.61683 \pm 0.013	0.283 \pm 0.064	0.134 \pm 0.027	0.01146 \pm 0.00074	0.01679 \pm 0.00080	0.3768 \pm 0.0038
2008-2009	0.828 \pm 0.020	0.75697 \pm 0.026	0.336 \pm 0.040	0.061 \pm 0.011	0.00437 \pm 0.00059	0.00801 \pm 0.00091	0.3810 \pm 0.0017
[†] 2009-2010	0.72174	0.64518	0.135	0.081	0.0079	0.0204	0.3869
2010-2011	0.610 \pm 0.036	0.54054 \pm 0.037	0.114 \pm 0.022	0.0265 \pm 0.0069	0.0124 \pm 0.0022	0.0198 \pm 0.0029	0.39563 \pm 0.00057
2013-2014	0.531 \pm 0.012	0.48492 \pm 0.012	0.234 \pm 0.020	0.104 \pm 0.014	0.02185 \pm 0.00060	0.02788 \pm 0.00065	0.3820 \pm 0.0024
2014-2015	0.634 \pm 0.016	0.52135 \pm 0.015	0.242 \pm 0.045	0.0170 \pm 0.0041	0.01436 \pm 0.00060	0.0233 \pm 0.0011	0.3949 \pm 0.0014
2015-2016	0.46 \pm 0.11	0.34875 \pm 0.12	0.099 \pm 0.035	0.0294 \pm 0.0048	0.0241 \pm 0.0060	0.049 \pm 0.012	0.3950 \pm 0.0021
2016-2017	0.602 \pm 0.034	0.4145 \pm 0.026	0.200 \pm 0.024	0.0450 \pm 0.0054	0.0182 \pm 0.0012	0.04530 \pm 0.00092	0.3858 \pm 0.0013

[†]With only 1 night observed it is not possible to evaluate uncertainties.

5. Discussing the relation between Ca and Fe

5.1. Implication for the Fe II/Fe I ionization ratio

Independently in both K and H line of the Ca II doublet, we measure an average absorption depth drop of about 0.36 ± 0.04 . The average K/H-line ratio of the dropped Ca II component is therefore about 1 ± 0.2 . Comparing the individuals AAD of K and H lines in Table 7 leads to a refined K/H ratio closer to 1.2. Thus, the Ca II varying medium is likely *not fully* saturated. In terms of equivalent width, with the core of the variation concentrated within $\pm 5 \text{ km s}^{-1}$ of β Pictoris velocity, we can estimate that

$$W_{K,H} = AAD \times \frac{10 \text{ km s}^{-1}}{c} \times \lambda_{K,H} \quad (1)$$

The lower limit from simple linear relation between equivalent width and column density in the K and H lines gives that the variation of the column density of Ca II should be $\Delta N_{\text{Ca II}} > 4.5 \cdot 10^{11} \text{ cm}^{-2}$. Using Somerville (1988) equivalent width ratio method, best to use in close-to-saturated cases, we find a range of possible column density for a ratio of 1.2:

$$\Delta N_{\text{Ca II}} \sim 1 - 4 \cdot 10^{12} \text{ cm}^{-2} \quad (2)$$

This should be compared to the $\Delta N_{\text{Fe I}} = (7.5 \pm 0.9) \cdot 10^{11} \text{ cm}^{-2}$ lost during the 2011-2013 drop in the ground level column density. Assuming that Ca is fully ionized below 1 au (Fernandez et al. 2006), we can obtain an estimation of the abundance of Ca with respect to Fe in this medium, by calculating $\Delta N_{\text{Ca II}} / \Delta N_{\text{Fe I}}$. We find a ratio of about

$$\text{Ca II/Fe I} \sim 1 - 5 \quad (3)$$

Therefore, Ca II and Fe I are almost as abundant in this medium. If it follows β Pic standard abundances (Roberge et al. 2006), with Fe/Ca ~ 15 , then we must have Fe II/Fe I $\sim 15-75$, implying a low ionization rate for Fe. This is in fairly good agreement with the results of VM17, proposing that Fe I/Fe II $\lesssim 1$ in the 20.4 km s^{-1} component at 1300 K.

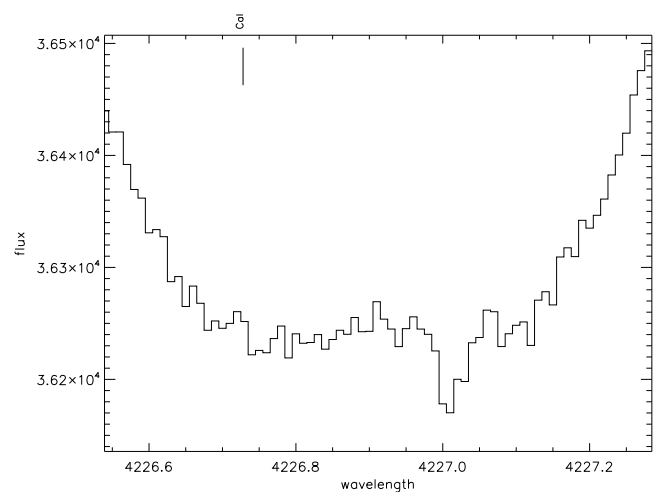


Fig. 7. Ca I absorption line at 4226.728 Å with a shift of 20 km s^{-1} . All HARPS spectra from 2003 to 2017 are here co-added.

5.2. Ca I line variations

In the HARPS spectra, we also found a Ca I circumstellar absorption line about 4226.728 Å, as plotted on Fig. 7. Measuring its variation allow comparing Ca I and Fe I and determining independently the Ca/Fe abundance ratio. We thus analysed as for Fe I the variation of the column density in this line using *Owens.f.* The results are given in Table 8, and compared to Fe I and Ca II variations in Fig. 8.

Again we found a $2\text{-}\sigma$ significant drop of column density compatible with 30% between 2011 and 2013. The measured column density variation is $\Delta N_{\text{Ca I}} = (1.54 \pm 0.70) \times 10^8 \text{ cm}^{-2}$. This means that Ca I, Ca II and Fe I variations are all compatible and most likely originate from a common medium.

First comparing the column density variation of Ca I, to the one estimated above for Ca II, we find that indeed Ca is almost fully ionized with a ratio Ca II/Ca I $\sim 10^4$, much higher than what primarily found by Hobbs et al. (1985) but closer to the theoretical estimations of Fernandez et al. (2006). Second, comparing this Ca I variation to $\Delta N_{\text{Fe I}}$ we find that Fe I is ~ 5000 (± 2400) times more abundant than

Table 8. The variation of the Ca I velocity shift, b value and column density evaluated by fitting the ground base line at 4226.728 Å. Upper-limits for b-values are given at 1-sigma.

Periods (year)	SNR	v (km s ⁻¹)	b (km s ⁻¹)	log N _{FeI} (cm ⁻²)
2003-2004	2120	19.80±0.25	<2.0	8.48±0.08
2004-2007	870	21.29±0.42	<1.4	8.60 ^{+0.10} _{-0.20}
2007-2008	1200	19.53±0.35	<1.00	8.52 ^{+0.10} _{-0.16}
2008-2009	1980	19.85±0.22	1.30±0.45	8.69±0.09
2009-2010	590	15.42 ^{+0.93} _{-0.67}	—	<8.25 [†]
2010-2011	860	19.56±0.63	<1.5	8.44 ^{+0.15} _{-0.43}
2013-2014	1350	20.08±0.45	<1.1	8.35 ^{+0.13} _{-0.25}
2014-2015	800	20.70±0.44	<1.6	8.66±0.15
2015-2016	950	31.40 ^{+0.35} _{-0.70}	—	<8.51 [†]
2016-2017	1450	20.35±0.65	<1.1	8.17 ^{+0.16} _{-0.63}

[†]2-sigma upper-limit calculated varying v in range 19-21 km s⁻¹.

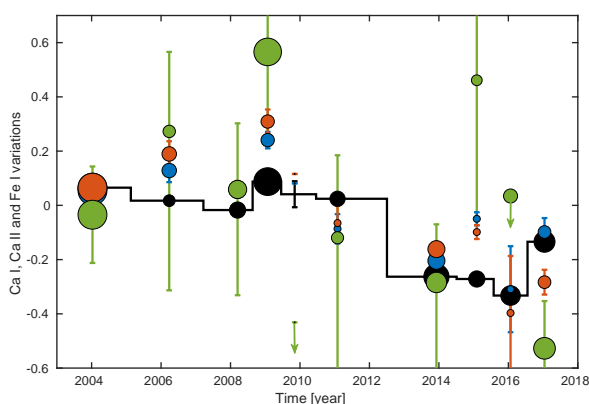


Fig. 8. Scaled-to-median Ca I column density variations at 4226.728 Å, in green, compared to Ca II-K (in blue), Ca II-H (in red) and Fe I variations (black). Absolute values for Ca I column densities are reported in Table 8. The median of all datasets was shifted to 0. The size is proportional to the number of observed nights for Ca II, while it is proportional to SNR for Fe I and Ca I, as given in Tables 7, 4 and 8 respectively.

Ca I. If originating from a common medium, then according to photoionisation-recombination balance (Lagrange et al. 1995), Ca and Fe should follow, at a given distance to the central star, a one-to-one correspondance in first ionization ratio

$$N_{\text{FeI}}/N_{\text{FeII}} = 200 \times N_{\text{CaI}}/N_{\text{CaII}} \quad (4)$$

Assuming that $N_{\text{Fe}} \sim N_{\text{FeII}}$ and $N_{\text{Ca}} \sim N_{\text{CaII}}$ is a fairly good approximation even if $\text{Fe II}/\text{Fe I} \sim 10$. In this case, we derive an abundance ratio Fe/Ca of about 25 (± 12). It is compatible with the solar value for this ratio ~ 15 (Lodders 2003, Lodders 2010) and the value found in β Pic by Roberge et al. (2006), 15 ± 10 .

We can also confirm that Fe ionisation ratio is low with the direct measurement of $\text{Fe II}/\text{Fe I} \sim 30-100$, using the above formula and the estimation of $N_{\text{CaI}}/N_{\text{CaII}}$.

6. Conclusion

To summarize the reported results, we observed in the circumstellar gas disk of β Pictoris that

- The Fe I ground level column density drop of 2011-2013 is also observed in the Fe I excited levels absorption lines centered around velocity 20.4 km s⁻¹,
- The blue and red components of Fe I₀ absorption lines have different variability, with the 20.4 km s⁻¹ more compatible with a sudden drop, while the blue component seems to have an independent behavior,
- We identified a varying Ca II component in the circumstellar line region, which equivalent width is dropping in average with an amplitude comparable to that of Fe I.
- The Ca I circumstellar line also experiences a drop between 2011 and 2013. This drop is compatible with β Pic-like relative abundances for Ca and Fe,
- The varying component of Fe has a low ionisation ratio, in agreement with VM17 results.

First we conclude that the VM17 1300 K medium at 20.4 km s⁻¹ contains not only Fe, but also Ca, and both stands at photoelectric equilibrium. It is located at close distance to the star $\sim 38 R_{\star}$ to sustain the 1300 K temperature and the high ionisation ratio of Ca. The Fe I blue component is likely not connected to this inner disk and belongs to a colder outer location with different photoionization conditions, possibly from recombination of Fe II beyond 100 AU, as described by Brandeker et al. (2004,2011).

Second, although the Ca II absorptions due to exocomets in the β Pictoris spectrum have a strong variability, they do not show any long term or sudden variations as in the column density of the 20.4 km s⁻¹ component of Fe I. On the other hand, depth variations in the core of the Ca II circumstellar line have a stronger compatibility with the Fe I drop. Large and slow transiting exocomets could be at the origin of such absorptions, blended within the circumstellar line, such as members of the D-family, as suggested by Welsh & Montgomery (2016). However, the absence of correlated variations at larger velocity (up to +30 km s⁻¹ in β Pic rest frame) where most D-family objects lie does not support this hypothesis.

Small scale disk inhomogeneities with yearly density variations are another alternative scenario. Such variations could be triggered by an outer planet, through direct gravitational interaction or indirectly by changing the flux of incoming dust within an inner disk at 0.3 au. However in that case a periodic behaviour would be expected. The baseline is not long enough to confirm or exclude periodicity, but a slight increase of the Fe I column density is already observed. The continuation of the monitoring of β Pic optical spectrum with high resolution spectrograph such as HARPS will allow testing this scenario.

Acknowledgements. We thank the anonymous referee for his help on greatly improving the quality of the article. We warmly thank T. Lanz for fruitful discussions on the subject of the present article. F.K. acknowledge support by a CNES fellowship grant. A.L.E., A.V-M and F.K thank the CNES for financial support. This work has been partly carried out thanks to an award from the Fondation Simone et Cino Del Duca. P.A.W. acknowledge support from the European Research Council under the European Unions Horizon 2020 research and innovation programme under grant agreement No. 694513. V. B. and D. E. acknowledge support by the Swiss National Science Foundation (SNSF) in the frame of the National Centre for Competence in Research PlanetS, and has received funding from the European Research Council (ERC) under the European Union's Horizon 2020 research and innovation programme (project Four Aces; grant agreement No 724427). HARPS data were obtained at ESO 3.6m telescope from 2003 to 2017, with Program IDs, 60.A-9036, 072.C-0636, 075.C-0234, 076.C-0073, 076.C-0279, 078.C-0209, 079.C-0170, 080.C-0032, 080.C-0664, 080.C-0712, 081.C-0034, 082.C-0308, 082.C-0412, 084.C-1039,

091.C-0456, 094.C-0946, 098.C-0739, 099.C-0205, 099.C-0599, 184.C-0815, & 192.C-0224

References

- Artymowicz, P., 1997, *Annual Review of Earth and Planetary Sciences*, 25, 175
- Backman, D. E., Paresce F., 1993, *Protostars and Planets III*, 1253
- Beust, H., Vidal-Madjar, A., Ferlet, R., & Lagrange-Henri, A. M. 1990, *A&A*, 236, 202
- Brandeker, A., Liseau, R., Olofsson, G., & Fridlund, M. 2004, *A&A*, 413, 681
- Brandeker, A. 2011, *ApJ*, 729, 122
- Ferlet, R., Vidal-Madjar, A., & Hobbs, L. M. 1987, *A&A*, 185, 267
- Fernández, R., Brandeker, A., & Wu, Y. 2006, *ApJ*, 643, 509
- Hébrard, G., Lemoine, M., Vidal-Madjar, A., et al. 2002, *ApJS*, 140, 103
- Hobbs, L. M., et al., 1985, *ApJ*, 293, L29
- Kiefer, F., Lecavelier des Etangs, A., Boissier, J., et al. 2014, *Nature*, 514, 462
- Lagrange, A. M., et al., 1995, *A&A*, 296, 499
- Lagrange A.-M., et al., 2012, *A&A*, 542, A18
- Lagrange, A.-M., et al., 2018, *A&A*, 612, A108
- Lecavelier des Etangs, A., Vidal-Madjar, A. & ferlet, R. 1996a, *A&A*, 307, 542L
- Lemoine, M., Vidal-Madjar, A., Hébrard, G., et al. 2002, *ApJS*, 140, 67
- Li A., Greenberg, J. M., 1998, *A&A*, 331, 291
- Lodders, K. 2003, *ApJ*, 1220, 591
- Lodders, K., 2010, *Astrophysics and Space Science Proceedings*, 16, 379
- Mamajek, E. E., Bell C. P. M., 2014, *MNRAS*, 445, 2169
- Pepe, F., Lovis, C., Ségransan, D., et al. 2011, *A&A*, 534, 58
- Roberge, A., Feldman, P. D., Weinberger, A. J., Deleuil, M. & Bouret, J.-C. 2006, *Nature*, 441, 724
- Smith, B. A. & Terrile, R. J. 1984, *Science*, 226, 1421
- Vidal-Madjar, A., Lecavelier des Etangs, A., & Ferlet, R. 1998, *Planet. Space Sci.*, 46, 629
- Vidal-Madjar, A., et al., 2017, *A&A*, 607, A25
- Weissman, P. R., 1984, *Science*, 224, 987
- Weissman, P. R., 1984, *Lunar and Planetary Science Conference*, 15, 904
- Welsh, B. Y., & Montgomery, S. L., 2016, *PASP*, 128, 064201